Materials & Design 207 (2021) 109859

Contents lists available at ScienceDirect

Materials & Design

journal homepage: www.elsevier.com/locate/matdes

Compliant curved-crease origami-inspired metamaterials with a programmable force-displacement response

Ting-Uei Lee [a,b,c,d], Yan Chen [a,b], Michael T. Heitzmann [e], Joseph M. Gattas [c,*]

[a] School of Mechanical Engineering, Tianjin University, Tianjin, China
[b] Key Laboratory of Mechanism and Equipment Design of Ministry of Education, Tianjin, China
[c] School of Civil Engineering, University of Queensland, St. Lucia, Australia
[d] Centre for Innovative Structures and Materials, School of Engineering, RMIT University, Melbourne, Australia
[e] School of Mechanical and Mining Engineering, University of Queensland, St. Lucia, Australia

HIGHLIGHTS

- A new type of compliant curved-crease origami-inspired metamaterial is proposed.
- Adopting an elastica non-zero principal curvature enables a predictable and programmable force–displacement response.
- Origami unit cell construction parameters can be used to generate a wide range of response shapes.
- A new curved-crease bending translation (CCBT) method is proposed for analytical response prediction.

GRAPHICAL ABSTRACT

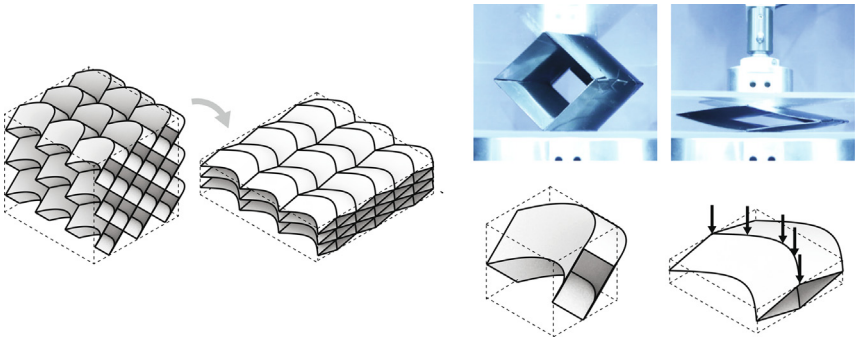

ARTICLE INFO

Article history:
Received 11 January 2021
Revised 24 May 2021
Accepted 31 May 2021
Available online 7 June 2021

Keywords:
Curved-crease origami
Compliant mechanism
Elastic bending
Metamaterial

ABSTRACT

Origami-inspired metamaterials utilise geometric sheet transformations to generate and control novel material mechanical properties. The majority of research effort has been devoted to straight-crease origami-inspired metamaterials, however curved-crease origami, which allows compliant folding and bending behaviours, has significant potential for adoption. This study proposes a new type of compliant curved-crease origami-inspired metamaterial, constructed with an 'elastica' non-zero principal surface curvature. Construction parameters for the new metamaterial are shown to influence a range of non-linear force–displacement response characteristics, including response shape, response duration, and response magnitude. A concise analytical curved-crease bending translation (CCBT) method is developed for rapid response prediction from metamaterial geometric parameters. The CCBT method also then enables the direct design and specification of a metamaterial with a fully programmable compliant force–displacement response.

1. Introduction

Origami-inspired metamaterials allow new mechanical properties to be artificially engineered, simply by folding a flat sheet. This fascinating ability has led to a new generation of adaptive materials and devices, with novel mechanical behaviours including tunable and graded structural stiffness [1,2], programmable deformations [3,4], negative Poisson's ratio [5–7], and multi-stability [8–10]. By drawing on the rich historical catalogue of artistic origami geometries, material engineers have found origami-inspired microstructures that offer enhanced deformabil-

* Corresponding author.
E-mail address: j.gattas@uq.edu.au (J.M. Gattas).

https://doi.org/10.1016/j.matdes.2021.109859
0264-1275/

ity, compactness, and lightness as compared to traditional lattice, chiral, or holey cellular metamaterials [11]. Corresponding applications have been suggested for energy-absorbing and resilient high-performance materials [12,13], and more broadly across a range of engineering disciplines including for acoustic metamaterials [14], sandwich structures [15], and DNA nanostructures [16].

The majority of origami-inspired metamaterials have been developed from straight-crease origami [17,18]. An example shown in Fig. 1(a)-(b) is formed by tessellating a tubular unit cell in three directions. The unit is formed from classic 'Miura-ori' straight-crease patterns, which follow a single degree-of-freedom rigid-foldable motion path, where panels remain flat and deformation only occurs by rotation about fold lines. There is thus a kinematic coupling between fold line rotations and unit cell volumetric variation, allowing Miura pattern parameters to be used for tailoring of the metamaterial mechanical response. Additional control can be attained from the strain energy storage capability in pattern fold lines [19]. Fold line rotational stiffness can be controlled from material selection and manufacturing method [20], with resting and self-stress states additionally controlled from annealing or plastic crease folding [21,22].

Curved-crease origami is an alternate class of origami patterns which possess a curved fold that imparts a non-zero principal curvature into a thin sheet during folding [23–26]. They are noted for their striking and beautiful folded forms and as such, are widely employed as decorative or aesthetic components, including as packaging, sculptures, and façades [27–29]. A classical method for construction of curved-fold developable surfaces is to reflect the parallel generators of a single-curved surface in an inclined mirror plane [23]. The reflected parallel generators form a second surface with equal and opposite curvature to the first, with the two surfaces connected by a planar 'fold-line' at their mirror plane intersection.

This study proposes a new type of compliant origami-inspired metamaterial, shown in Fig. 1(c)-(d), with a curved-crease unit cell constructed with an 'elastica' non-zero principal surface curvature. Elastica curves are the elastically-deformed shapes of a straight slender beam [30,31] and when employed for curved-crease construction, have been shown to generate an equilibrated minimum-energy surface [32]. Experimental and numerical simulations of the compressed metamaterial show the parameters used in unit cell construction allow complete control over response shape, duration, and magnitude. A new *curved-crease bending translation* (CCBT) method is proposed for analytical response prediction, allowing a predictable and programmable force–displacement response from metamaterial construction parameters.

2. Materials and methods

2.1. Cellular geometry

For metamaterial specification, a tubular unit cell volume is defined with height H, breadth B, and length L parameters, as shown in Fig. 2(a). It is composed of two curved-crease origami, connected at mid-height along non-developable crease lines [33]. Each origami has a single curved crease, formed from reflection of a curved surface at the top or bottom XY faces of the unit cell volume, and creating a topology similar to the curved-crease Miura-ori pattern [34]. The curved surface is constructed with a non-zero principal curvature adopted as an elastica curve, with arc length S and deformed width $b = B$ sufficient for its definition [35,36]. The internal angle between surface generators at developable and non-developable crease lines is η_A and η_B, respectively, with $\eta_B = \pi/2 - \eta_A/2$. Total folded edge length is $W = 2H/\sin\eta_B$ and the surface is unfolded to two $S \times W/2$ sheets to form the crease patterns required for manufacture. Tessellation of the unit cell gives a complete metamaterial with T_x, T_y, and T_z cells in lateral, longitudinal, and vertical directions, respectively.

2.2. Specimen design

To explore compliant folding behaviours of the proposed curved-crease metamaterial, a parametric experimental study was conducted on specimens with varied unit cell construction and cell tessellation parameters. Eight specimen types were devel-

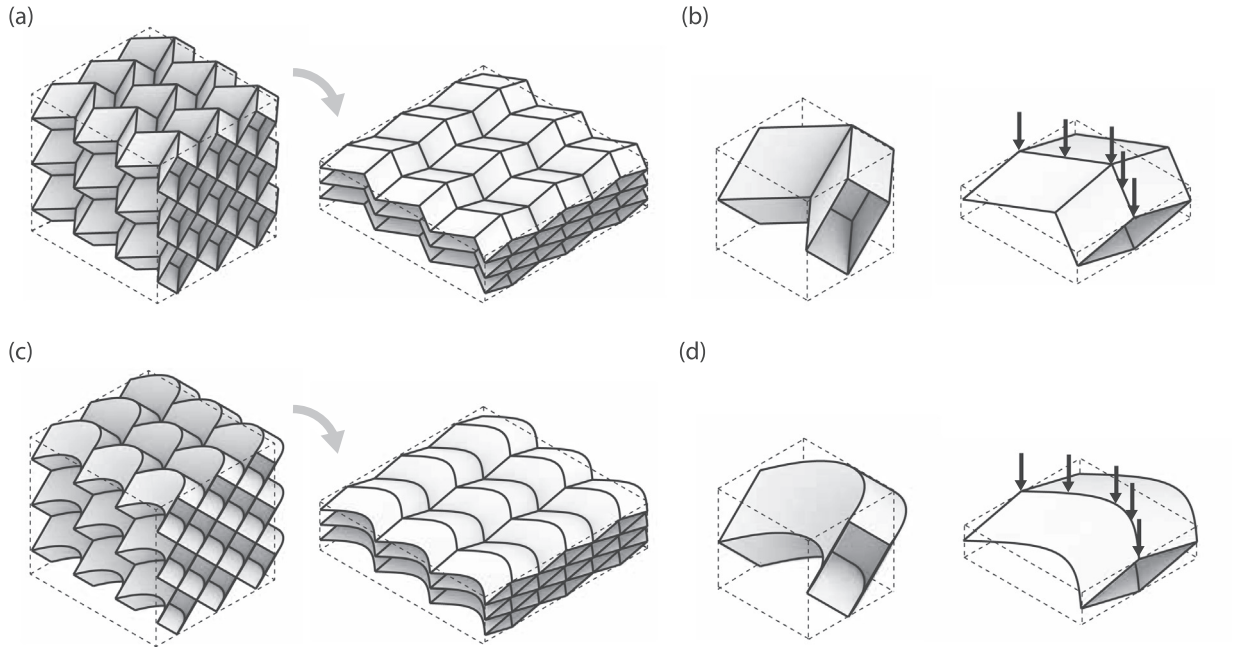

Fig. 1. Origami-inspired metamaterials. (a) Undeformed and deformed straight-crease tessellated metamaterial. (b) Undeformed and deformed straight-crease unit cell. (c) and (d) Curved-crease metamaterial and unit cell.

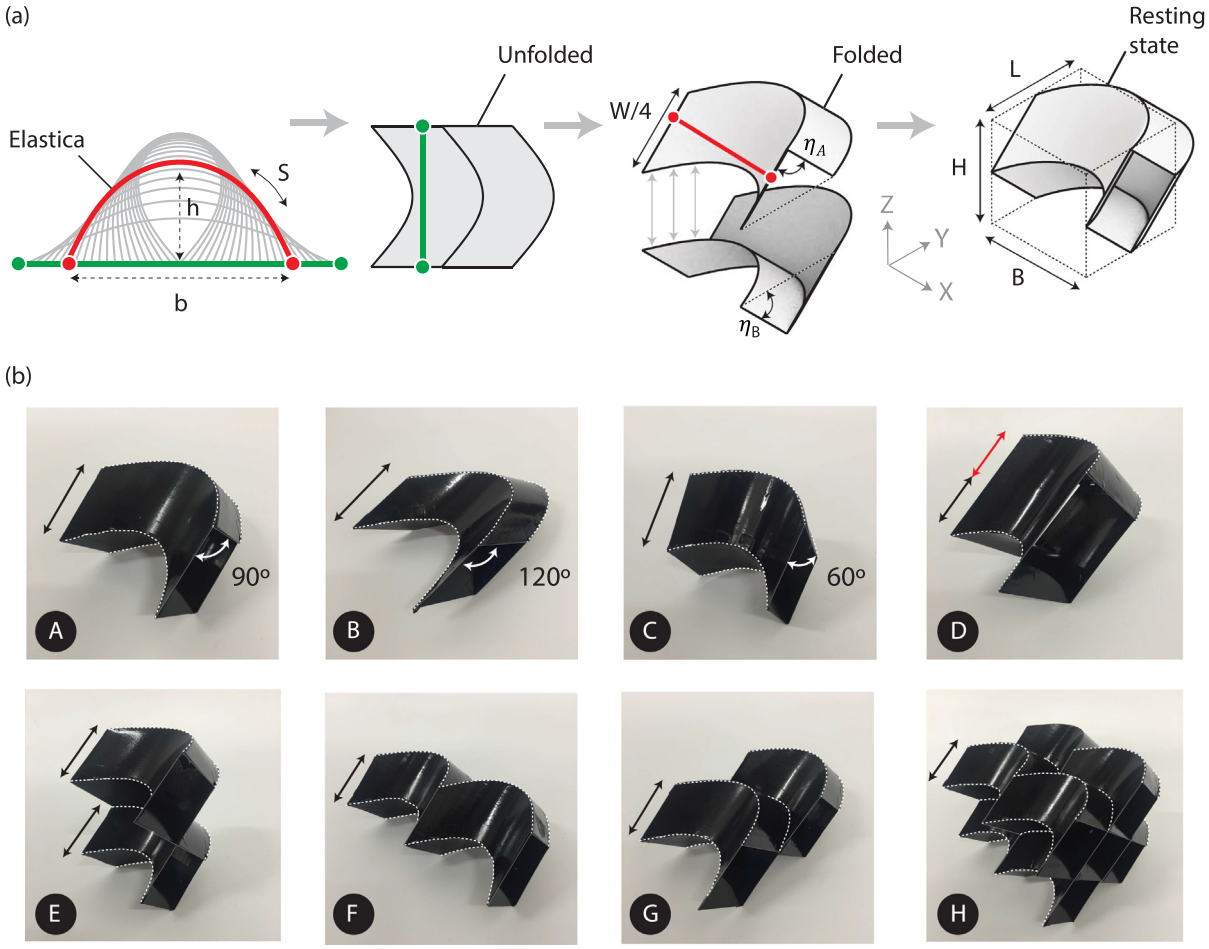

Fig. 2. Unit cell specification. (a) Geometric construction and (b) eight parametric study configurations.

Table 1
Specimen parameters and FE/EXP/CCBT comparisons.

Specimen	Resting-state: $H' = 0$					Near-flat				
	$W \times S$ (mm)	b/S (–)	η_A (°)	H (mm) (mm)	(T_x, T_y, T_z) (–)	H' (mm)	b/S (–)	U_{FE} (mJ)	U_{EXP} (mJ)	U_{CCBT} (mJ)
(A)	180 × 90	0.75	90	63.64	(1,1,1)	15.64	0.99	89.70	87.19	90.33
(B)	180 × 90	0.75	**120**	**45**	(1,1,1)	11.00	0.99	74.24	73.09	83.54
(C)	180 × 90	0.75	**60**	**77.94**	(1,1,1)	18.94	0.99	101.16	96.80	100.36
(D)	**360** × 90	0.75	90	**127.28**	(1,1,1)	31.28	0.99	167.39	157.61	180.66
(E)	180 × 90	0.75	90	**127.28**	**(1,1,2)**	31.28	0.99	187.71	164.59	180.66
(F)	180 × 90	0.75	90	63.64	**(2,1,1)**	15.64	0.99	183.47	184.04	180.66
(G)	180 × 90	0.75	90	63.64	**(1,2,1)**	15.64	0.99	183.54	182.16	180.66
(H)	180 × 90	0.75	90	**127.28**	**(2,2,2)**	31.28	0.99	756.02	692.05	722.63

oped as shown in Fig. 2(b), with parameters summarised in Table 1.

The base specimen (A) was used for generation of other specimen types, with systematic variation of metamaterial construction parameters to ascertain their influence over response characteristics. A first specimen set evaluated the influence of origami edge angle construction parameter η_A, between adjacent curved surfaces at developable crease lines. Specimens (A), (B), and (C), were specified with η_A = 90°, 120°, and 60°, respectively. Elastica cross-section and origami tessellation parameters were otherwise the same between the three specimen types.

A second specimen set evaluated the influence of construction parameters influencing metamaterial height. Specimens (D) and (E) both have twice the height of base specimen (A); (D) has a doubled edge length $2W$ and (E) contains two units stacked in an out-of-plane tessellation, $T_z = 2$. A third specimen set evaluated the influence of in-plane unit cell tessellation on response behaviour. Specimens (F) and (G) contain two units arranged as in-plane tessellations $T_x = 2$ and $T_y = 2$, respectively. Specimen (H) has 8 units with a grid tessellation of $T_x = T_y = T_z = 2$.

2.3. Fabrication

Experimental specimens were fabricated from a 0.5 mm thick isotropic PET sheet, with individual component panels cut,

annealed, and joined such that the volumetric form of the metamaterial was its resting state, and the flattened configuration was its stressed state. The fabrication process is shown in Fig. 3 and summarised as follows.

Panel components were laser cut from a planar sheet, bent, and placed into an ABS 3D printed mould with the designed elastica profile. The mould assembly was then heated at a constant temperature of 79°C for one hour in an oven, to allow thermal annealing and stress relief in the bent PET panels, without impacting the ABS mould. Component panels were removed from the mould and cooled to room temperature, before being joined together with a 0.1 mm thick vinyl hinge. The hinge type was selected as possessing a very small rotational stiffness but with sufficient translational connectivity to resist the separation of parts during folding. The hinge layer was attached to a single face of panels. The face was selected to allow panels to open and close freely during folding, as highlighted in Fig. 3, to minimise edge contact and maintain an approximately near-zero rotational stiffness in crease lines.

2.4. Testing and numerical modelling

Prototypes were subjected to a uniaxial quasi-static compression test in a Type 5982 Instron Universal Testing Machine, as shown in Fig. 4(a). The specimens were compressed at a rate of 60 mm/min and until 75–80% of their original height, as shown in Fig. 4(b)-(c), with force and displacement measured at the Instron cross-head. Force response was not recorded during unloading, however all tested unit cells were observed to return to their initial shape, with no visible permanent deformation.

The compliant mechanical response of the compressed unit cell was simulated with a finite element (FE) analysis in commercial software Abaqus. A modelling approach for simulation of curved-crease origami with low rotational-stiffness crease line regions was developed previously and is fully described in [37], but is summarised briefly here as follows.

Surfaces were meshed with S4 shell elements and an approximate mesh size of 1 mm, set following a convergence study. Surface thickness was 0.5 mm, except at crease lines which were modelled as 0.5 mm wide regions with a reduced thickness of 0.05 mm. An implicit nonlinear quasi-static analysis method was used to allow for large deformation geometric nonlinearity. Mechanical properties for the PET sheet were obtained from material tensile tests, with the obtained stress–strain curves showing a linear-like elastic behaviour with Young's modulus E = 2299 MPa and fracture point at approximately 50 MPa. For FE simulations, the material was assumed as linear elastic, as stress remained well within the elastic region. The model was compressed between two external rigid plates, with displacement control applied to the top plate and a hard normal contact between all surfaces.

3. Results and discussion

3.1. Parametric response investigation

Force–displacement paths for the first specimen set (A), (B), and (C), designed with varying edge angle parameter η_A, are shown in Fig. 5(a)-(c). A significant feature can be observed from specimen responses: the metamaterial *response shape* is substantially altered across the three specimens. The base specimen (A) with η_A = 90° shows an approximately uniform and stable response, that is an 'elastic–plastic' response shape, noting however that it is achieved here via elastic bending of the constituent panel material. Specimen (B) with η_A = 120° shows a 'hardening' response shape and specimen (C) with η_A = 60° shows a 'softening' response shape. All specimens were observed to be near-fully compressible, up to 75% of their respective heights.

FE predictions are consistent with experimental results, and showed an unfolding and energy behaviour for all specimens similar to that shown in Fig. 4(b). As the specimen is compressed, component panels gradually flatten and expand in the transverse directions due to a kinematic coupling from the developable crease lines. As panel curvature reduces, metamaterial internal energy U arises primarily from elastic bending strain energy. A shell buckling behaviour, as circled in red in Fig. 4(c), is also observed in some specimens as they approach a near-flat configuration. This will be discussed further in the next section.

Force–displacement paths for the second specimen (A), (D), and (E), constructed with varying height, are shown in Fig. 5(d)-(f). It can be seen that *response duration* has approximately doubled in specimens (D) and (E), but that the response shape is otherwise the same as for specimen (A). The response of (E) is remarkably similar to (D), indicating that tessellated unit cells transmitted the folding motion across their adjoining crease line. FE results

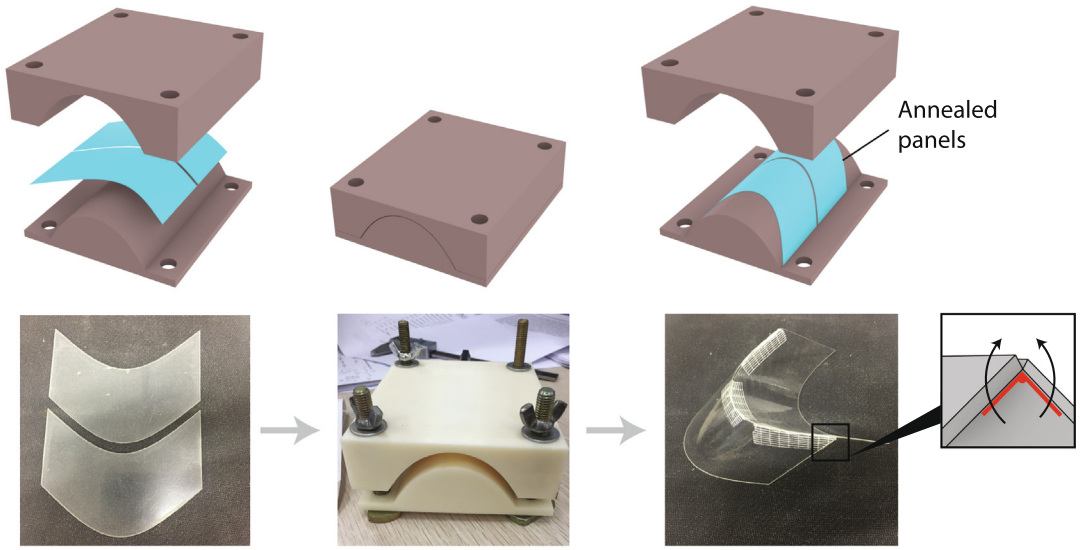

Fig. 3. Unit cell fabrication. Component panels were cut and annealed at the designed curvature. Curved panels were joined to resist the separation of parts during folding.

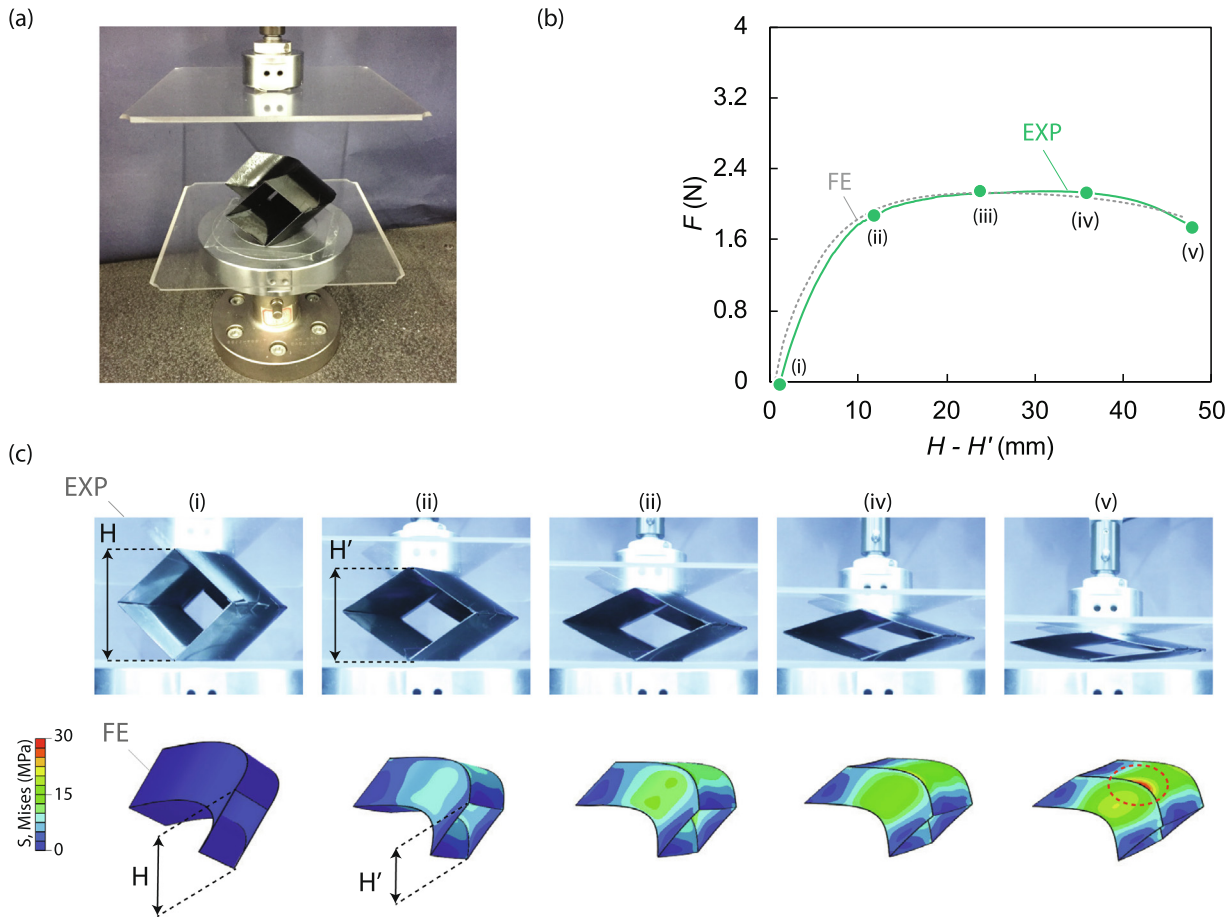

Fig. 4. Unit cell testing and simulation. (a) Experimental set-up, (b) experimental and FE response comparison, and (c) deformation sequence comparison.

show that the internal energy U for (D) and (E) was approximately double that of (A). For specimen (E), bending strain energy was also approximately the same in top and bottom unit cells.

Force–displacement paths for the third specimen set (A), (F), (G), and (H), constructed with varied unit cell tessellation, are shown in Fig. 5(g)-(i). It can be seen that *response magnitude* for specimens (F) and (G) are approximately twice that for specimen (A), with response duration unchanged. Their responses are also almost identical, indicating a smooth in-plane expansion across adjoining crease lines in both directions. The response magnitude for specimen (H) is approximately four times that of specimen (A), with response duration also doubled due to the out-of-tessellation. From FE models, the internal energy U for specimens (F)/(G) and (H) are shown to have an approximately two or eight times the energy of base specimen (A), as summarised in Table 1.

To summarise the findings from the second and third specimen groups, the curved-crease unit cell can be considered as a non-linear mechanical spring, with in-plane and out-of-plane metamaterial tessellations causing a parallel or series behaviour, respectively. In-plane tessellations have a parallel spring behaviour which amplifies energy and response magnitude, without changing the response duration. Out-of-plane tessellations have a series spring behaviour which amplifies energy and response duration, without changing response magnitude.

3.2. Curved-crease bending translation (CCBT) method

This paper proposes a new *curved-crease bending translation* (CCBT) method for prediction of the force–displacement response of elastica-generated curved-crease metamaterials. The method evaluates a 'local' energy-displacement response by assuming an elastica motion path for deformed panel cross-sectional curvatures. It then translates this local behaviour to a 'global' energy-displacement response, using origami kinematic relationships.

3.2.1. Local energy-displacement response

Elastica curves represent the minimum energy response of elastically-bent 1D slender rods. They have been extensively studied for a range of boundary conditions and deformations. For example, the 2D elastica curves plotted in Fig. 6(a) are attained from analytical solutions [35,36] and represent the intermediate bent states of a rod with a fixed central boundary condition, deformed from h to h'.

The curved-crease metamaterial unit cells are composed of four panels with identical reflected curvatures in the undeformed state, as specified by an initial elastica curve. The CCBT method assumes that the reflected curvatures of the four panels remain identical in any deformed state, and that these deformed curvatures correspond to the idealised deformed shapes of a 2D elastica rod. This correspondence occurs in a 'local' cross-sectional plane perpendicular to the linear surface generators as shown in Fig. 6(a). As aligned in this plane, a 2D slender rod with properties equivalent to component panels will have length S, depth t, and width $4 \times W/4 = W$.

Initial and deformed states have curvatures, κ and κ', respectively, obtained from analytical elastica solutions. The elastic bending strain energy U at the deformed state can be evaluated from the change in curvature as [38,39]:

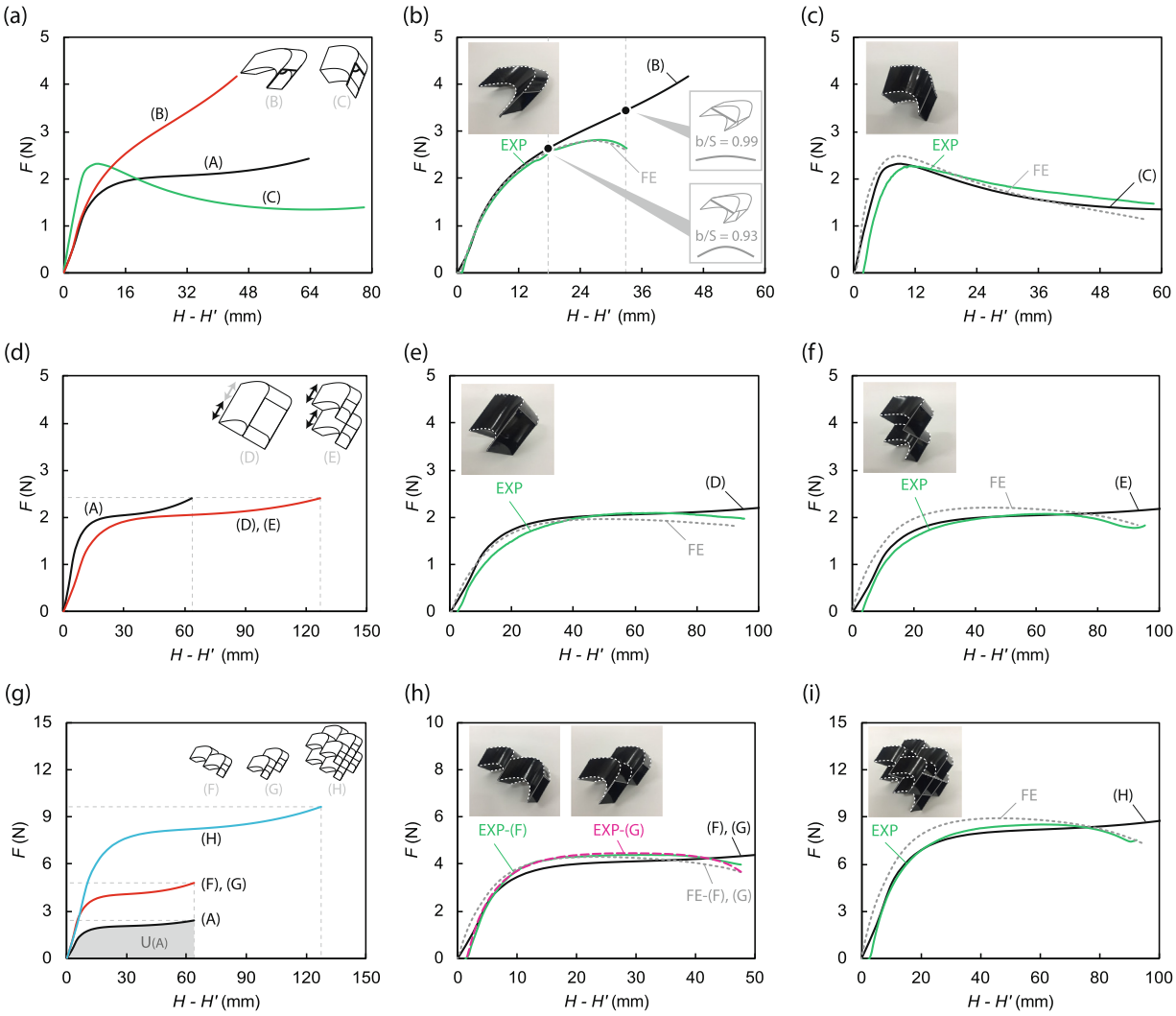

Fig. 5. Parametric investigation results. CCBT prediction in left column and FE/EXP/CCBT comparisons in middle and right columns. (a)-(c) Response shape specimens A-C. (d)-(f) Response duration specimens D and E. (g)-(i) Response magnitude specimens F-H.

$$U = \frac{EI}{2}\int_S (\kappa - \kappa')^2 ds \tag{1}$$

where $0 \leqslant s \leqslant S, I = Wt^3/12$, and E is the material elastic modulus. A 'local' energy-displacement response is obtained by evaluating Eq. 1 across a full local displacement history, from an undeformed $h' = h$ state to a fully-flat $h' = 0$ state. The evaluated local energy response is shown in Fig. 6(c), with U plotted against change in local height $(h - h')$.

3.2.2. Global energy-displacement response

The assumption of identical deformed panel curvatures introduces additional simplifications related to crease line and panel behaviour. First, crease lines are assumed to perfectly enforce translational connectivity, have zero size, and remain planar during folding. Second, a planar crease requires that generators of deformed panels would remain parallel and collinear throughout the folding process [23,40]. Kinematically, these assumptions create a rigid-foldable planar-quadrangle mesh which can be used to directly simulate folding motion [17,41], however they also allow for certain kinematic relationships to be established for translation of the local displacement h' to a global displacement H'.

With reference to Fig. 6(b), in the undeformed state, parameter w_k describes the perpendicular distance from the panel boundary edge to nearest cross-sectional frame, as measured along the central generator line. This can be calculated from unit cell construction parameters as:

$$w_k = \frac{h}{\tan \eta_B} \tag{2}$$

Under the above assumptions, w_k is invariant across deformed states, so Eq. 2 can be rearranged to solve deformed edge angle from local displacement:

$$\eta_B' = \tan^{-1}\left(\frac{h'}{w_k}\right) \tag{3}$$

Deformed edge angle and deformed unit cell height are related as:

$$H' = \frac{W}{2}\sin \eta_B' \tag{4}$$

With substitution of Eq. 3 into 4, global displacement can be expressed directly as a function of local displacement and geometric construction constants:

$$H' = \frac{W}{2}\frac{1}{\sqrt{1 + \left(\frac{w_k}{h'}\right)^2}} \tag{5}$$

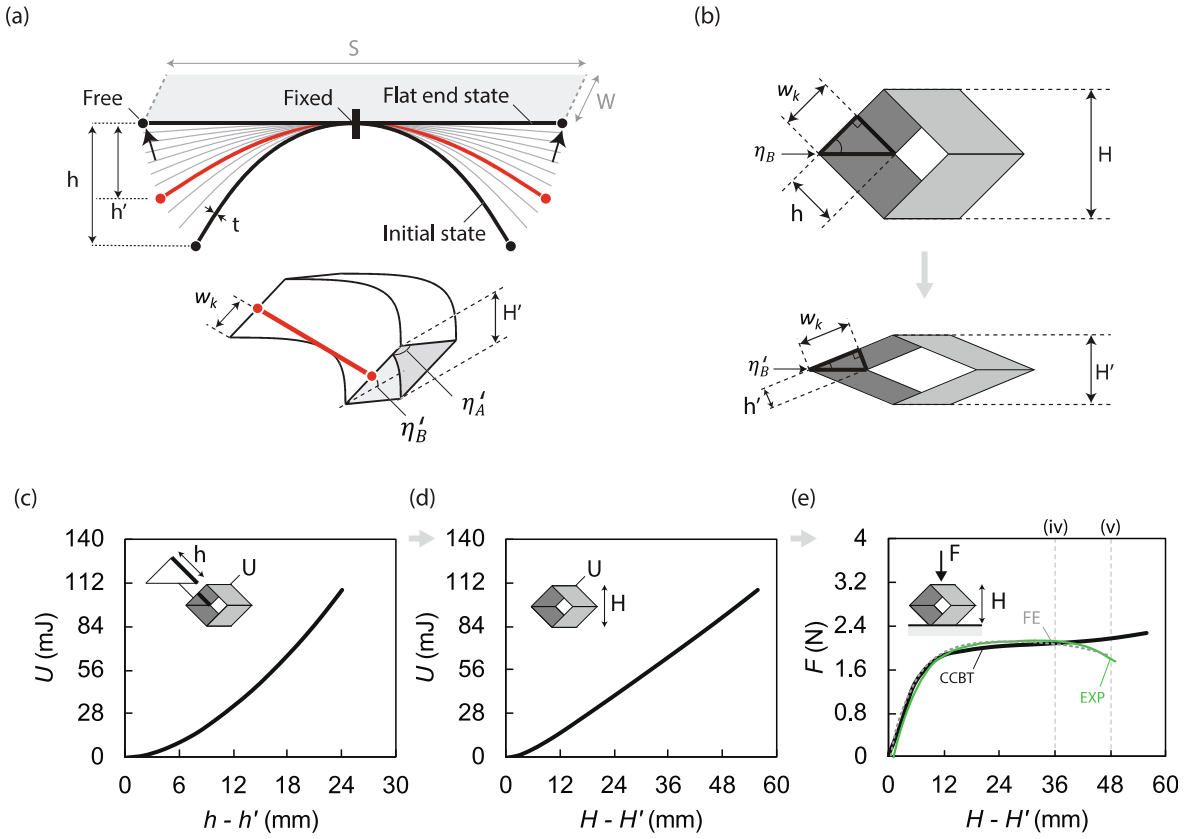

Fig. 6. Curved-crease bending translation (CCBT) method. (a) Intermediate folded states and parameters. (b) Local to global translation parameters. (c) Local energy-displacement, (d) global energy-displacement, and (e) global force–displacement responses.

Eq. 5 allows the local energy-displacement response plotted against $(h - h')$ to be converted to a global energy-displacement response plotted against $(H - H')$, shown in Fig. 6(d). The derivative of energy with respect to deformed distance $(H - H')$ in the global-Z direction gives the final unit cell force–displacement response as:

$$F = \frac{dU}{dH'} \tag{6}$$

which is plotted in Fig. 6(e).

3.2.3. Method verification

For CCBT method implementation, elastica profiles were evaluated from $0 \leqslant h'/h \leqslant 100\%$ at 5% increments, with profiles obtained using existing analytical solutions for one-dimensional simply-supported beams [35,36]. Tangent angles and curvature were evaluated at 100 sampling points along each profile, for numerical integration of Equation 1 and evaluation of local strain energy. Equations 5–6 were then used for translation to a global force–displacement response.

Experimental and numerical results for the base specimen (A) from Fig. 4(b) are re-plotted in Fig. 6(e) alongside its CCBT response prediction. It can be seen that there is a good agreement over the majority of the response history, which confirms the underlying CCBT assumption of elastica bending behaviour being preserved across component panels in deformed states. The CCBT response is seen to deviate over the indicated region from (iv)-(v), when the local cross-section is approaching a near-flat configuration at $b/S \approx 0.98$–0.99, respectively. This region corresponds to onset of shell buckling and stress concentration observed in numerical models around the crease-line region, shown in Fig. 4(c), which invalidates the underlying assumptions of the CCBT model. This edge buckling likely arises due to several complex factors, including edge loading of the component panels, complex stress transfer across the crease line, and non-transverse stress states arising from the shell material Poisson effect and non-rectangular crease line boundaries.

CCBT predictions for other tested metamaterial configurations are shown in Fig. 5. For in-plane metamaterial tessellations (F)-(H), the CCBT unit cell response was multiplied by the number of unit cells and for out-of-plane metamaterial tessellations (F) and (I) the tessellated global displacement was divided uniformly across unit cell layers. Good correspondence is seen for all configurations. Shell buckling onset and CCBT prediction deterioration is also seen for most cases and is influenced most strongly by the edge angle construction parameter η_A. Specimen (B) with $\eta_A = 120^\circ$ has the earliest deterioration at $b/S \approx 0.93$, whereas specimen (C) with $\eta_A = 60^\circ$ shows minimal deterioration up to $b/S \approx 0.99$. The edge angle influence is consistent with the above-identified factors likely contributing to a shell edge buckling behaviour. As the developed fabrication and testing procedure is unsuited to closer investigation of this phenomenon, further study is out-of-scope for the present paper.

The CCBT method is concluded to be effective in enabling rapid prediction of the non-linear force–displacement response across a wide range of curved-crease metamaterial configurations, particularly over initial and intermediate deformed states. The proposed metamaterial is however a restricted class of curved-crease origami, in that it is a pattern with an orthogonal in-plane tessellation and an elastica-generated principal design curvature. The CCBT method could potentially be adapted for curved-crease origami patterns constructed with other elastica solutions, for example

higher-order elastica curves [32], with slight variation to assumptions used in formation of the local energy response. However, the relationships formulated for translation to a global displacement reference frame are only valid for in-plane tessellations with an out-of-plane actuation, applied uniformly across all constituent unit cells.

3.3. Response analysis and design

3.3.1. Response shape analysis

The CCBT method can be used to gain insight into the response shape variation observed for specimens (A)-(C), as influenced by the origami edge angle construction parameter. Of the translation steps introduced in the previous section, the energy (U) - local displacement $(h - h')$ response is the same for all specimens, as they were constructed with the same elastica curvature. The geometric influence over response shape must therefore arise from the translation from the local h' to global H' displacement reference frame, Eq. 5. This is plotted in Fig. 7(b) for specimens (B), (A), and (C), with η_B = 30°, 45°, and 60°, respectively. Specimen force–displacement responses are also reproduced from Fig. 5(a) in Fig. 7(a), for reference.

From Fig. 7(b), it can be seen that specimen (C) has a higher initial rate of change of h' with H', as compared to other specimens. That is, a small initial global compression $(H - H')$ will generate a larger compression in the local cross-sectional plane $(h - h')$, and thus a larger curvature change and strain energy release. Conversely, as specimen (C) approaches the fully-compressed state, it has a lower rate of change and thus lower strain energy release as compared to other specimens. This can be seen more clearly by normalising global compression along the x-axis to $0 \leqslant (H - H')/H \leqslant 100\%$, Fig. 7(c), and also by plotting dh'/dH' directly, Fig. 7(d). dh'/dH' is obtained as the product of $dh'/d\eta'_B$ and $d\eta'_B/dH'$, derived from Eqs. 3 and 4, respectively, as:

$$\frac{dh'}{d\eta'_B} = w_k \sec^2 \eta'_B \tag{7}$$

$$\frac{d\eta'_B}{dH'} = \frac{1}{\frac{dH'}{d\eta'_B}} = \frac{2}{W} \sec \eta'_B \tag{8}$$

and plotted in Figs. 7(e)-(f). Combined, these give:

$$\frac{dh'}{dH'} = \frac{dh'}{d\eta'_B}\frac{d\eta'_B}{dH'} = \frac{2w_k}{W} \sec^3 \eta'_B \tag{9}$$

as plotted in Figs. 7(d). From Eq. 9, specimens with a higher initial η_B will have an initial amplification in dh'/dH' due to the $\sec^3 \eta'_B$ term. However they will also have an overall reduction in dh'/dH' by the scalar factor $2w_k/W$, with $w_k \propto 1/\tan \eta_B$ as per Eq. 2.

This complex geometric interaction has a convenient outcome for the purposes of overall response shape control. Considering specimen (B), its lower η_B gives a lower initial dh'/dH' and higher final dh'/dH', Fig. 7(d). This causes a reasonably linear h' to H' translation, Fig. 7(c), and an overall force–displacement response that corresponds to the geometric stiffening occurring from panel bending in local system, Fig. 7(a). The inverse is seen in specimen (C), with its higher η_B giving a higher initial dh'/dH' and lower final dh'/dH'. This shifts the overall force–displacement response towards a softening response, with rapid initial and slower final panel bending in the local system.

3.3.2. Programmable response

A programmable global force–displacement response can be realised from the insight gained into the effect of curved-crease metamaterial design parameters. The following four design steps are proposed to specify the nine design parameters, $\eta_A, W, S, b/S, E, t, T_x, T_y$, and T_z, for attainment of a target metamaterial response. The process is illustrated in Fig. 8.

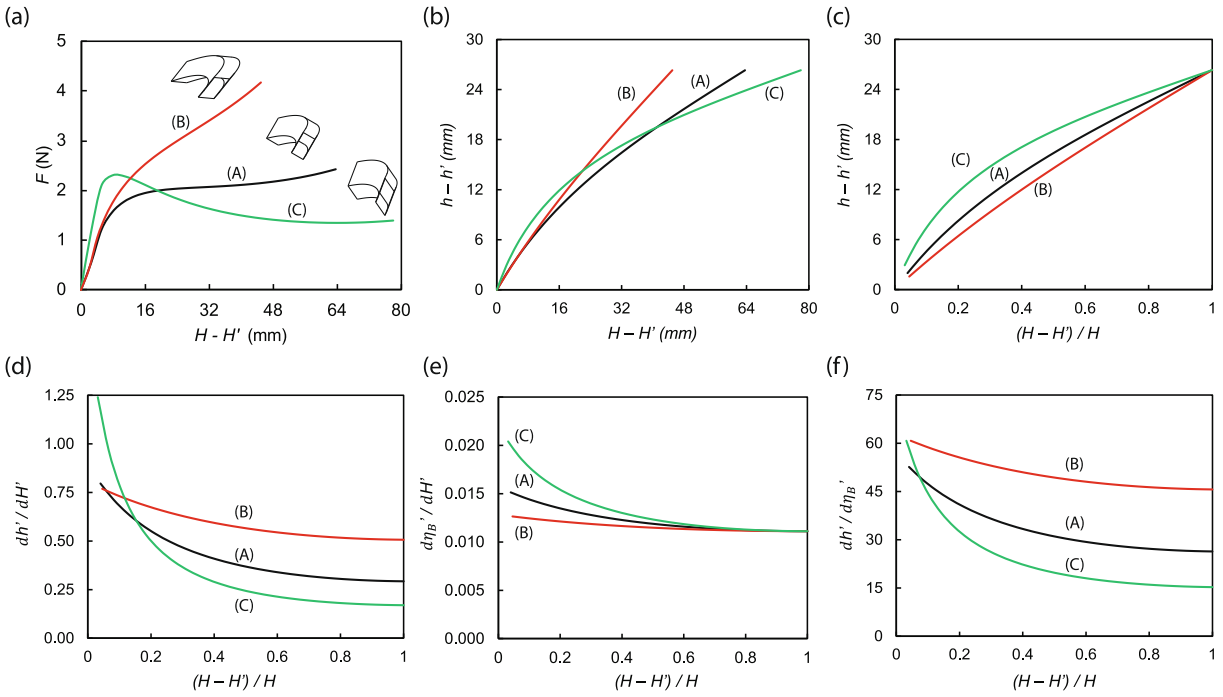

Fig. 7. Response shape analysis. (a) Response shape variation in specimens (A)-(C). (b)-(c) Local versus global displacement translation. (d) Rate of change of h' with H', obtained as the product of (e) $d\eta'_B/dH'$ and (f) $dh'/d\eta'_B$.

1. Select the global force–displacement *response type* by modifying the edge angle η_A curved-crease unit cell.
2. Determine the global force–displacement *response duration* by modifying the unit cell height H through edge length W and/or out-of-plane tessellation T_z.
3. Define the *elastic strain energy potential* U of a desired unit cell by adjusting elastica cross-section design parameters S and b/S and/or material properties E and t, calculated using Eq. 1.
4. Amplify the *response magnitude* for the tessellated metamaterial with in-plane tessellation T_x and/or T_y.

3.4. Comparison with existing mechanical metamaterials

The curved-crease metamaterial demonstrates two highly novel and beneficial mechanical response attributes, unavailable in current cellular and straight-crease origami topologies: i) precise control over the material's response shape; and ii) an ultra-resilient elastic deformation behaviour whereby the entire material can be near-fully compressed with no permanent distortion.

Response shape control has only previously been observed in 'holey sheet' cellular mechanical metamaterials, which comprise a slab of elastomer, embedded with a periodic array of holes or pore shapes. Their nonlinear stress–strain behaviour arises from buckling in the cell microstructure wall, with propagating collapse bands causing a pattern transformation and change in response shape. Numerical optimisation is typically required to program and optimise the response shape due to its generation from a complex elastic instability and pattern switch behaviour [42]. In contrast, there is no elastic instability in the proposed curved-crease metamaterial, with the response arising purely from large elastic

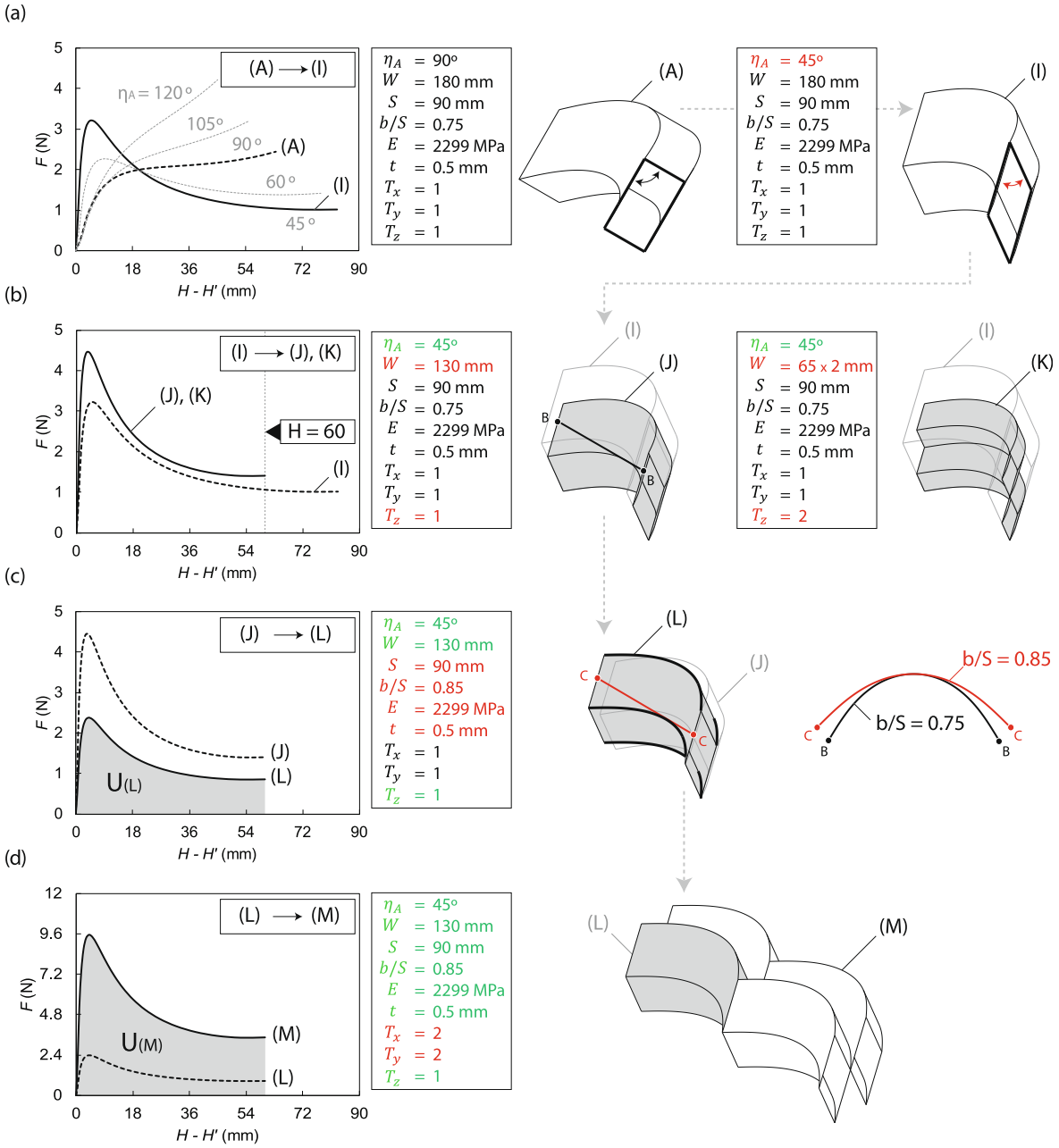

Fig. 8. Programmable force–displacement response. (a) Response shape. (b) Response duration. (c) Unit cell strain energy potential. (d) Response magnitude.

bending of the constituent curved panels, across the entire material. This enables precise, direct control over response shape, from unit cell geometric design parameters.

The proposed curved-crease metamaterials also allow for complete elastic recoverability at exceptionally high compressive strains, recorded as up to 80% of material height in the tested specimens. This is significantly higher than current resilient metamaterials, for example hierarchical nanolattice metamaterials which also have near-complete height recoverability but only up to 50% compressive strain [43].

Straight-crease origami metamaterials also can allow for high elastic compression and recovery, but as their energy contribution arises from small elastic hinge areas, they will likely have a much lower energy density than the proposed curved-crease materials with energy contribution from large elastic panel areas. Consider for example the straight-crease unit cell of Fig. 1(b), constructed with a similar panel thickness, weight, and volume to the investigated curved-crease unit cell. Straight-crease deformation is typically assumed as rigid-foldable motion, with deformation occurring via hinge rotation. However this requires hinge bending stiffness to be substantially smaller than panel bending stiffness, with a large corresponding reduction in hinge line strain energy storage capability.

4. Conclusion

This study investigated the compliant folding behaviour of a curved-crease origami metamaterial. A range of non-linear force–displacement responses were generated and validated with numerical and experimental comparisons. It was found that the metamaterial response shape can be controlled through pattern edge angle parameter at its resting state η_A; response duration can be controlled through the alternation of pattern edge length W and/or out-of-plane tessellation T_z; and response magnitude can be controlled through in-plane tessellations T_x and T_y. Moreover, out-of-plane tessellation, in-plane tessellation, and combined tessellation manifest as a series, parallel, and combined non-linear mechanical spring effects, respectively.

An elastica motion path was shown to represent the deformed cross-sectional surface curvature of the proposed curved-crease unit cell, with crease lines acting to enforce uniform deformation across all panels in a tessellated metamaterial. The proposed CCBT method converted this elastica local energy-displacement response to a global force–displacement response prediction, to concisely and rapidly predict a range of metamaterial response features. By extension, a curved-crease metamaterial can be rapidly designed with the CCBT method to possess a fully programmable force–displacement response. The method has however only been studied for one class of elastica-generated curved-crease origami, with further research needed to investigate whether it can be extended to other curved-crease origami topologies.

Data availability

Supplementary data to this article can be found online at https://doi.org/10.14264/d56e35e.

Declaration of Competing Interest

The authors declare that they have no known competing financial interests or personal relationships that could have appeared to influence the work reported in this paper.

Acknowledgements

The authors gratefully acknowledge the financial support provided by the Australian Research Council Discovery Project DP160103279 and the National Natural Science Foundation of China (project numbers 51825503, 51721003 and 51575377).

References

[1] E.T. Filipov, T. Tachi, G.H. Paulino, Origami tubes assembled into stiff, yet reconfigurable structures and metamaterials, Proc. Nat. Acad. Sci. 112 (40) (2015) 12321–12326.
[2] J. Ma, J. Song, Y. Chen, An origami-inspired structure with graded stiffness, Int. J. Mech. Sci. 136 (2018) 134–142.
[3] E.T. Filipov, G. Paulino, T. Tachi, Origami tubes with reconfigurable polygonal cross-sections, Proceedings of the Royal Society A: Mathematical, Physical and Engineering Sciences 472 (2185) (2016) 20150607.
[4] Q. Zhang, J. Wommer, C. O'Rourke, J. Teitelman, Y. Tang, J. Robison, G. Lin, J. Yin, Origami and kirigami inspired self-folding for programming three-dimensional shape shifting of polymer sheets with light, Extreme Mechanics Letters 11 (2017) 111–120.
[5] M. Schenk, S.D. Guest, Geometry of miura-folded metamaterials, Proc. Nat. Acad. Sci. 110 (9) (2013) 3276–3281.
[6] H. Yasuda, J. Yang, Reentrant origami-based metamaterials with negative poisson's ratio and bistability, Phys. Rev. Lett. 114 (18) (2015) 185502.
[7] G. Sossou, F. Demoly, H. Belkebir, H.J. Qi, S. Gomes, G. Montavon, Design for 4d printing: Modeling and computation of smart materials distributions, Materials & Design 181 (2019) 108074.
[8] J.L. Silverberg, A.A. Evans, L. McLeod, R.C. Hayward, T. Hull, C.D. Santangelo, I. Cohen, Using origami design principles to fold reprogrammable mechanical metamaterials, Science 345 (6197) (2014) 647–650.
[9] S. Kamrava, D. Mousanezhad, H. Ebrahimi, R. Ghosh, A. Vaziri, Origami-based cellular metamaterial with auxetic, bistable, and self-locking properties, Scientific Reports 7 (2017) 46046.
[10] F. Bobbert, S. Janbaz, T. van Manen, Y. Li, A. Zadpoor, Russian doll deployable meta-implants: Fusion of kirigami, origami, and multi-stability, Materials & Design (2020) 108624.
[11] X. Yu, J. Zhou, H. Liang, Z. Jiang, L. Wu, Mechanical metamaterials associated with stiffness, rigidity and compressibility: A brief review, Prog. Mater Sci. 94 (2018) 114–173.
[12] S.E. Calisch, Folded functional foams, Ph.D. thesis, Massachusetts Institute of Technology (2019).
[13] K. Liu, L.S. Novelino, P. Gardoni, G.H. Paulino, Big influence of small random imperfections in origami-based metamaterials, Proceedings of the Royal Society A 476 (2241) (2020) 20200236.
[14] P.P. Pratapa, P. Suryanarayana, G.H. Paulino, Bloch wave framework for structures with nonlocal interactions: Application to the design of origami acoustic metamaterials, J. Mech. Phys. Solids 118 (2018) 115–132.
[15] A.L. Wickeler, H.E. Naguib, Novel origami-inspired metamaterials: Design, mechanical testing and finite element modelling, Materials & Design 186 (2020) 108242.
[16] P. Wang, S. Gaitanaros, S. Lee, M. Bathe, W.M. Shih, Y. Ke, Programming self-assembly of dna origami honeycomb two-dimensional lattices and plasmonic metamaterials, J. Am. Chem. Soc. 138 (24) (2016) 7733–7740.
[17] X. Zhou, S. Zang, Z. You, Origami mechanical metamaterials based on the miura-derivative fold patterns, Proceedings of the Royal Society A: Mathematical, Physical and Engineering Sciences 472 (2191) (2016) 20160361.
[18] J. Zhang, D. Karagiozova, Z. You, Y. Chen, G. Lu, Quasi-static large deformation compressive behaviour of origami-based metamaterials, Int. J. Mech. Sci. 153 (2019) 194–207.
[19] K. Liu, G.H. Paulino, Nonlinear mechanics of non-rigid origami: an efficient computational approach, Proceedings of the Royal Society A: Mathematical, Physical and Engineering Sciences 473 (2206) (2017) 20170348.
[20] S.S. Tolman, I.L. Delimont, L.L. Howell, D.T. Fullwood, Material selection for elastic energy absorption in origami-inspired compliant corrugations, Smart Mater. Struct. 23 (9) (2014) 094010.
[21] Y. Klett, Paleo: Plastically annealed lamina emergent origami, in: ASME 2018 International Design Engineering Technical Conferences and Computers and Information in Engineering Conference, American Society of Mechanical Engineers, 2018, pp. V05BT07A062–V05BT07A062.
[22] S.W. Grey, F. Scarpa, M. Schenk, Mechanics of paper-folded origami: A cautionary tale, Mech. Res. Commun. (2020) 103540.
[23] J.P. Duncan, J. Duncan, Folded developables, Proceedings of the Royal Society of London. A. Mathematical and Physical Sciences 383 (1784) (1982) 191–205.
[24] Y. Liu, H. Pottmann, J. Wallner, Y.-L. Yang, W. Wang, Geometric modeling with conical meshes and developable surfaces, in: ACM transactions on graphics (TOG), Vol. 25, ACM, 2006, pp. 681–689.
[25] M.A. Dias, L.H. Dudte, L. Mahadevan, C.D. Santangelo, Geometric mechanics of curved crease origami, Phys. Rev. Lett. 109 (11) (2012) 114301.
[26] M.A. Dias, B. Audoly, A non-linear rod model for folded elastic strips, J. Mech. Phys. Solids 62 (2014) 57–80.

[27] M. Schein, Applied generative procedures in furniture design, in: Proceedings of the Generative Art International Conference, 2002, pp. 21–1.
[28] E.D. Demaine, M.L. Demaine, D. Koschitz, Reconstructing David Huffman's legacy in curved-crease folding, Origami 5 (2011) 39–52.
[29] G. Epps, S. Verma, Curved folding: Design to fabrication process of robofold, Shape Modeling International 2013 (2013) 75.
[30] L. Euler, Methodus inveniendi lineas curvas maxima minimive proprietate gaudentes additamentum i, De Curvis Elasticis, Lausanne and Geneva 1744.
[31] C.L. Dym, I.H. Shames, et al., Solid Mechanics, Springer, 1973.
[32] T.-U. Lee, Z. You, J.M. Gattas, Elastica surface generation of curved-crease origami, International Journal of Solids and Structures.
[33] K.A. Seffen, Compliant shell mechanisms, Philosophical Transactions of the Royal Society A: Mathematical, Physical and Engineering Sciences 370 (1965) (2012) 2010–2026.
[34] K. Miura, Zeta-Core Sandwich- Its Concept and Realization, Institute of Space and Aeronautical Science, University of Tokyo, 1972.
[35] A. Valiente, An experiment in nonlinear beam theory, Am. J. Phys. 72 (8) (2004) 1008–1012.
[36] Q. Pacheco, E. Piña, et al., The elastic rod, Revista Mexicana de Física E 53 (2) (2007) 186–190.
[37] T.-U. Lee, Y. Chen, J.M. Gattas, Curved-crease origami with multiple states, in: Origami 7: Seventh International Meeting of Origami Science, Mathematics, and Education, CRC Press, 2018, pp. 849–964.
[38] M. Kuijvenhoven, P. Hoogenboom, Particle-spring method for form finding grid shell structures consisting of flexible members, Journal of the International Association for Shell and Spatial Structures 53 (1) (2012) 31–38.
[39] J.C. Badger, T.G. Nelson, R.J. Lang, D.M. Halverson, L.L. Howell, Normalized coordinate equations and an energy method for predicting natural curved-fold configurations, Journal of Applied Mechanics 86 (7).
[40] K.A. Seffen, Spherical images and inextensible curved folding, Phys. Rev. E 97 (2) (2018) 023004.
[41] J.M. Gattas, Z. You, Miura-base rigid origami: parametrizations of curved-crease geometries, Journal of Mechanical Design 136 (12).
[42] A. Ghaedizadeh, J.H. Shen, X. Ren, M. Xie, Geometric bounds for buckling-induced auxetic metamaterials undergoing large deformation, in: Applied Mechanics and Materials, Vol. 846, Trans Tech Publ, 2016, pp. 547–552.
[43] L.R. Meza, A.J. Zelhofer, N. Clarke, A.J. Mateos, D.M. Kochmann, J.R. Greer, Resilient 3d hierarchical architected metamaterials, Proc. Nat. Acad. Sci. 112 (37) (2015) 11502–11507.